Synthesis and Crystal Structure Determination of Bifunctional Phosphine-Linked Triplatinum Double-Cluster Complexes

Daniel Imhof,† Urs Burckhardt,† Klaus-Hermann Dahmen,*,†,‡ Felix Joho,† and Reinhard Nesper†

Laboratorium für Anorganische Chemie, ETH, Zürich, Switzerland, and Department of Chemistry and MARTECH, The Florida State University, Tallahassee, Florida 32306-3006

Received July 18, 1996⊗

Reactions of $[Pt_3(\mu\text{-}CO)_3(PCy_3)_3]$ (**1**) and $[Pt_3(\mu\text{-}CNXyl)_2(\mu\text{-}CO)(CNXyl)(PCy_3)_2]$ (**2**) (Cy = C_6H_{11}, Xyl = C_8H_9) with $^1/_2$ equiv of a bifunctional metal phosphine cation $[(MPR'_2)_2(R)]^{2+}$ (M = Cu, Ag, Au; R = C_6H_4, $(CH_2)_2C_6H_4$, $Fe(C_5H_5)$; R′ = C_6H_5, C_6H_{11}) yielded quantitatively $[\{Pt_3(\mu\text{-}CO)_3(PCy_3)_3\}_2\{(MPR'_2)_2(R)\}]^{2+}$ and $[\{Pt_3(\mu\text{-}CNXyl)_2(\mu\text{-}CO)(CNXyl)(PCy_3)_2\}_2\{(MPR'_2)_2(R)\}]^{2+}$, respectively. The compounds were characterized by IR-, MS-, and ^{31}P-NMR spectroscopy. The X-ray structure is given for $[\{Pt_3(\mu\text{-}CO)_3(PCy_3)_3\}_2\{(AuPPh_2)_2(CH_2)_2C_6H_4)\}][PF_6]_2$ (**14**), which crystallizes in the triclinic space group $P\bar{1}$ with $Z = 1$, $a = 15.350$ Å, $b = 17.150$ Å, $c = 20.446$ Å, $\alpha = 84.54°$, $\beta = 84.84°$, and $\gamma = 64.56°$. The structure was refined to $R = 0.0435$ for the 8430 observed reflections ($I > 3\sigma(I)$).

Introduction

Trinuclear platinum clusters such as $[Pt_3(\mu\text{-}CO)_3(PR_3)_3]$, $[Pt_3(\mu\text{-}CNR)_2(\mu\text{-}CO)(CNR)(PR_3)_2]$, $[Pt_3(\mu\text{-}CNR)_3(CNR)_2(PR_3)]$, and $[Pt_3(\mu\text{-}SO_2)_{3-x}(\mu\text{-}L)_x(PR_3)_3]$ (L = CNXyl, Cl, SO_2, CO) can form heterometallic clusters by reaction with many metal-containing units, ML (Table 1).[1−16]

In order to understand qualitatively the bonding ability of the triplatinum clusters, the most important frontier orbitals must be considered, Scheme 1. The formation of heterometallic clusters can be explained by HOMO−LUMO interaction of the Pt_3 cluster and the heterometallic unit or vice versa. Thus the resulting products can be considered "Lewis acid−base addition" compounds. Different structures schematically drawn (types I−III) such as the half-sandwich type I or the sandwich type II

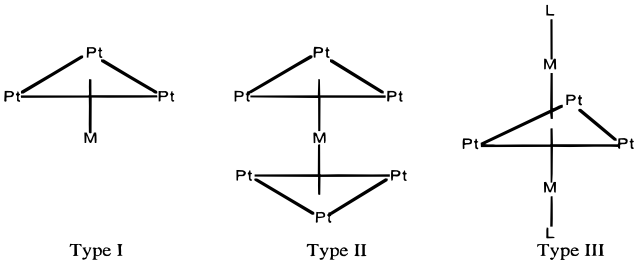

were found, in which the metal center is linked to one or two cluster units. Furthermore, a bicapped type III is known in which the Pt_3 building block is capped by a metal fragment ML on both sides.

Many of these compounds can be successfully used as precursors in heterogeneous catalysis.[17,18] Recently we found that $[Pt_3(\mu\text{-}CO)_3(PR_3)_3]$ and its heterometallic derivatives are active catalysts in the dehydrogenation of methylcyclohexane to toluene.[19]

Moreover, triangular clusters such as $[Pt_3(\mu\text{-}CO)_3(CO)_3]^{2-}$ can stack to clusters $[Pt_3(\mu\text{-}CO)_3(CO)_3]_n^{2-}$, $n = 1-10$, which show an extraordinary redox behavior that depends on the stacking size.[20]

Due to their geometric arrangement and "electron buffer abilities" clusters may be considered as useful building blocks for the systematic approach to molecular networks and macromolecules.

In principle there are three possible pathways to combine two Pt_3 units: (1) surface linking, (2) terminal ligand linking, and (3) bridge ligand linking (Figure 1).

This approach is not new; e.g., Vahrenkamp and co-workers have used bifunctional phosphines such as PPh_2RPPh_2 (R = p-C_6H_4 or 4,4′-C_6H_4-C_6H_4) for the preparation of double

* Author to whom correspondence should be addressed at Florida State University.
† ETH-Zürich.
‡ Florida State University (new address).
⊗ Abstract published in *Advance ACS Abstracts*, March 15, 1997.

(1) Albinati, A.; Dahmen, K.-H.; Togni, A.; Venanzi, L. M. *Angew. Chem.* **1985**, *97*, 760.
(2) Imhof, D.; Burckhardt, U.; Dahmen, K.-H.; Rüegger, H.; Gerfin, T.; Gramlich, V. *Inorg. Chem.* **1993**, *32*, 5206.
(3) Bhaduri, S.; Sharma, K.; Jones, P. G.; Erdbrugger, C. F. *J. Organomet. Chem.* **1987**, *329*, C46.
(4) Bour, J. J.; Kanters, R. P. F.; Schlebos, P. P. J.; Bosman, W. P.; Behm, H.; Beurskens, P. T.; Steggerda, J. J. *J. Organomet. Chem.* **1987**, *329*, 405.
(5) Braunstein, P.; Freyburger, S.; Bars, O. *J. Organomet. Chem.* **1988**, *352*, C29.
(6) Briant, C. E.; Wardle, R. W. M.; Mingos, D. M. P. *J. Organomet. Chem.* **1984**, *267*, C49.
(7) Dahmen, K.-H. Thesis, ETH 8172, 1986.
(8) Hallam, M. F.; Mingos, D. M. P.; Adatia, T.; McPartin, M. *J. Chem. Soc., Dalton Trans.* **1988**, 355.
(9) Hill, C. M.; Mingos, D. M. P.; Powell, H.; Watson, M. J. *J. Organomet. Chem.* **1992**, *441*, 499.
(10) Mingos, D. M. P.; Wardle, R. W. M. *J. Chem. Soc., Dalton Trans.* **1986**, 73.
(11) Mingos, D. M. P.; Oster, P.; Sherman, D. J. *J. Organomet. Chem.* **1987**, *320*, 257.
(12) Payne, N. C.; Ramachandran, R.; Schoettel, G.; Vittal, J. J.; Puddephatt, R. J. *Inorg. Chem.* **1991**, *30*, 4048.
(13) Stockhammer, A.; Dahmen, K.-H.; Gerfin, T.; Gramlich, V.; Peter, W.; Venanzi, L. M. *Helv. Chim. Acta* **1991**, *74*, 989.
(14) Ezomo, O. J.; Mingos, D. M. P.; Williams, I. D. *J. Chem. Soc., Chem. Commun.* **1987**, 924.
(15) Albinati, A.; Dahmen, K.-H.; Demartin, F.; Forward, J. F.; Longley, C. J.; Mingos, D. M. P.; Venanzi, L. M. *Inorg. Chem.* **1992**, *31*, 2223.
(16) Albinati, A.; Moor, A.; Pregosin, P. S.; Venanzi, L. M. *J. Am. Chem. Soc.* **1982**, *104*, 7672.
(17) Müller, S. Thesis, ETH 11160, 1995.
(18) Braunstein, P.; Bender, R.; Kervennal, J. *Organometallics* **1982**, *1* (9), 1236.
(19) Ichikawa, M. *J. Chem. Soc., Chem. Commun.* **1976**, 11.
(20) Longoni, P.; Chini, P. *J. Am. Chem. Soc.* **1976**, *98* (23), 7225.

S0020-1669(96)00846-4 CCC: $14.00

Table 1. Trinuclear Clusters Which Can Form Heterometallic Clusters by Reaction with Many Different Metal-Containing Units

building block {B}	Lewis-acid/-base	product	type	ref
$[Pt_3(\mu\text{-}CO)_3(PR_3)_3]$	$MPR_3^{+\,a}$	$[\{B\}\{MPR_3\}]^+$	I	6
$[Pt_3(\mu\text{-}CO)_3(PR_3)_3]$	$M^{+\,a}$	$[\{B\}_2M]^+$	II	1, 8
$[Pt_3(\mu\text{-}CO)_3(PR_3)_3]$	$MX_n^{\,b}$	$[\{B\}\{MX_n\}]^+$	II	13
$[Pt_3(\mu\text{-}CO)_3(PR_3)_4]$	$MPR_3^{+\,a}$	$[\{B\}\{MPR_3\}]^+$	II	3−5
$[Pt_3(\mu\text{-}Cl)(SO_2)_2(PR_3)_3]$	$AuPR_3^+$	$[\{B\}\{AuPR_3\}_2]^+$	III	11
$[Pt_3(\mu\text{-}CNXyl)(SO_2)_2(PR_3)_3]$	$AuPR_3^+$	$[\{B\}\{AuPR_3\}]^+$	II	9
$[Pt_3(\mu\text{-}CNR)_x(\mu\text{-}CO)_{3-x}(CNR)_y(PR_3)_{3-y}]^c$	$MPR_3^{+\,a}$	$[\{B\}\{MPR_3\}]^+$	II	2
$[Pt_3(\mu\text{-}CO)_3(PR_3)_3]$	Hg(0)	$[\{B\}_2Hg]$	I	16
$[Pt_3(\mu\text{-}CO)_3(PR_3)_3]$	Tl(I)	$[\{B\}Tl]^+$	II	14
$[Pt_3(\mu\text{-}CO)_3(PR_3)_3]$	Hg_2X_2	$[\{B\}\{HgX\}_2]$	III	15

[a] M = Cu(I), Ag(I), Au(I). [b] MX_n = ZnX_2, CdX_2, InX_3. [c] $x = 2$, $y = 1$, or $x = 3$, $y = 2$.

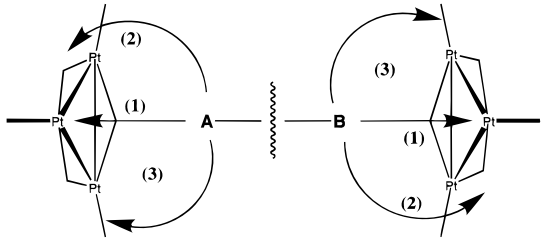

Figure 1. The three possible pathways to combine two Pt_3 units via (1) cluster-surface linking, (2) terminal ligand linking, and (3) bridge ligand linking.

Scheme 1

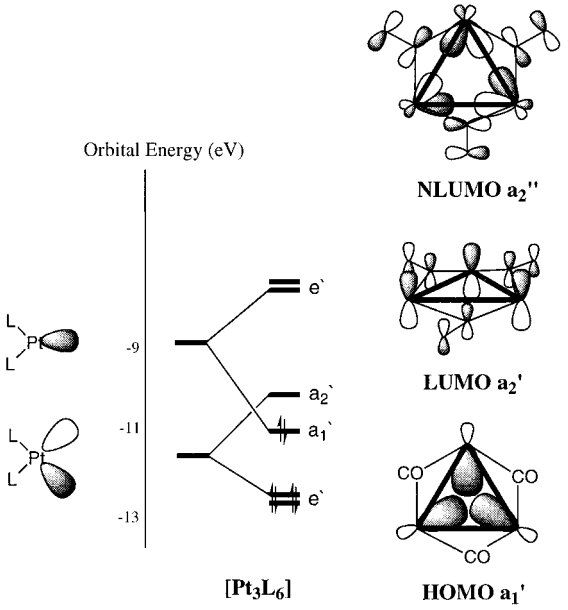

clusters.[21] In their research they have used $Co_3(CO)_9$, $FeCo_2(CO)_9$, $HFe_2Co(CO)_9$, and $H_2Fe_3(CO)_9$ as M_3 units.

In this paper we will discuss the synthesis and charaterization of bifunctional phospine-linked triplatinum clusters $[Pt_3(\mu\text{-}CO)_3(PR_3)_3]$, $[Pt_3(\mu\text{-}CNR)_2(\mu\text{-}CO)(CNR)(PR_3)_2]$, and $[Pt_3(\mu\text{-}CNR)_3(CNR)_2(PR_3)]$ (Figure 2).

Results

Phosphines. For the preparation of double (two cluster units per molecule) and triple clusters (three cluster units per molecule) appropriate bi- and trifunctional phosphines had to be synthesized with a delocalizable electronic system and a rigid molecular structure that cannot chelate the metal center. Numerous phosphine ligands fulfill these requirements.[22,23] In order to study the structural and electronic behavior, we prepared

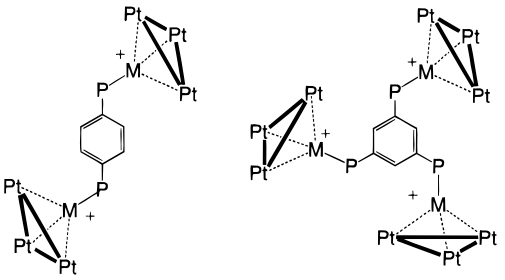

Figure 2. Cluster systems using delocalizable organometallic molecules as bridging units between the Pt_3 clusters.

bifunctional phosphines with cyclohexyl and phenyl groups (Figure 3).

While the phosphines **38** and **42** were synthesized according to the literature via a Birch reaction,[22] **39**−**41** and **43** were prepared via the corresponding PR_2Cl or PR_2H with R = Ph and Cy.[24,25]

These compounds were characterized by elemental analysis and IR- and ^{31}P-NMR spectroscopy. Chemical shifts of the ^{31}P-NMR spectra for all isolated bi- and trifunctional phosphines are given in the Experimental Section.

Gold, Copper, and Silver Phosphine Cations. The copper and silver phosphine cations were synthesized directly from the reaction of $Cu(CH_3CN)_4PF_6$ and $AgBF_4$ with the bifunctional phosphines. The gold phosphine cations were synthesized *in situ* by addition of $TlPF_6$ to the gold phosphine chlorides $[1,4\text{-}(AuClPPh_2)_2C_6H_4]$ (**44**), $[1,4\text{-}(AuClPCy_2)_2C_6H_4]$ (**45**), $[1,4\text{-}(AuClPPh_2CH_2)_2C_6H_4]$ (**46**), $[1,4\text{-}(AuClPCy_2CH_2)_2C_6H_4]$ (**47**), $[1,3,5\text{-}(AuClPPh_2)_3C_6H_3]$ (**48**), and $[1,1'\text{-}(AuClPPh_2)_2Fe(\eta\text{-}C_5H_5)_2]$ (**49**). All gold phosphine chlorides were synthesized according to the literature[26] by reducing $NaAuCl_4{\cdot}2H_2O$ with thiodiglycol. While older methods[27,28] used an excess of phosphine, as both a reagent and as reducing agent, this is unnecessary in the current method which leads to high yields of pure gold phosphine chlorides. They were identified by elemental analysis and IR and ^{31}P-NMR spectroscopy. The ^{31}P-NMR chemical shifts of these compounds are given in the Experimental Section.

Double/Triple Clusters. Just as the Lewis acids $CuPR_3^+$, $AgPR_3^+$, and $AuPR_3^+$ (*in situ*) react with $[Pt_3(\mu\text{-}CO)_3(PCy_3)_3]$ (**1**) and $[Pt_3(\mu\text{-}CNXyl)_2(\mu\text{-}CO)(CNXyl)(PCy_3)_2]$ (**2**) to give the addition products of type I,[2,6] the bifunctional copper, silver, and gold phosphine cations form the analogous double and triple

(21) Honrath, U.; Shu-Tang, L.; Vahrenkamp, H. *Chem. Ber.* **1985**, *118*, 132.

(22) McFarlane, H. C. E.; McFarlane, W. *Polyhedron* **1988**, *7*, 1875.
(23) Cotton, F. A.; Hong, B. *Prog. Inorg. Chem.* **1992**, *40*, 179.
(24) Baldwin, R. A.; Chen, M. T. *J. Org. Chem.* **1966**, *32*, 1572.
(25) Herring, D. L. *J. Org. Chem.* **1961**, *26*, 3998.
(26) Sutton, B. M.; McGusty, E.; Walz, D. T.; Dimartino, M. *J. Med. Chem.* **1972**, *15*, 1095.
(27) McAuliffe, C. A.; Parish, R. V.; Randall, P. D. *J. Chem. Soc., Dalton Trans.* **1979**, 1730.
(28) Carioti, F.; Naldini, L.; Simonetta, G.; Malatesta, L *Inorg. Chim. Acta* **1967**, *1*, 315.

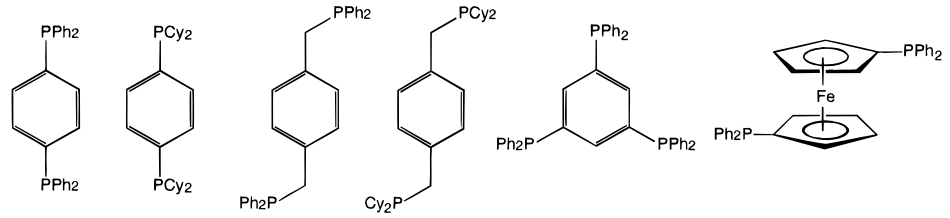

Figure 3. Bi- and trifunctional phosphines with cyclohexyl and phenyl groups.

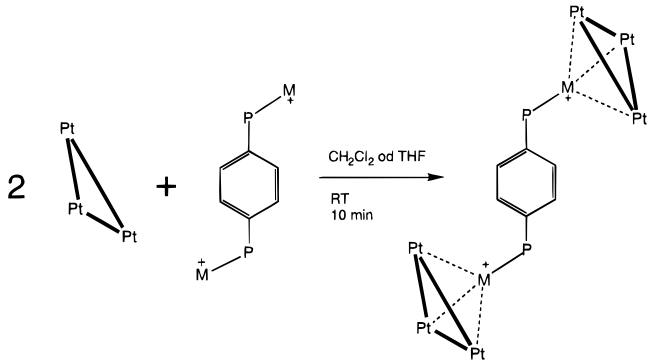

Figure 4. Synthesis of double and triple clusters.

Table 2. All the Compounds That Have Been Synthesized in This Study

Pt_3—M—PR'$_2$—R—PR'$_2$—M—Pt_3									
		Pt_3:	**1** [1)]			**2** [2)]			**22** [3)]
R	R'	M:	Cu	Ag	Au	Cu	Ag	Au	Au
	Ph		**3**	**4**	**5**	**6**	**7**	**8**	**23**
	Cy		**9**	**10**	**11**				
	Ph		**12**	**13**	**14**				
	Cy		**15**	**16**	**17**	**18**	**19**	**20**	**24**
	Ph				**21**				
	Ph		**25**	**26**	**27**				
Pt_3—M—PR'$_3$									
	Ph		**28**	**29**	**30**				
	Cy		**31**	**32**	**33**	**34**	**35**	**36**	**37**

clusters. For $[Pt_3(\mu\text{-CNXyl})_3(CNXyl)_2(PCy_3)]$ (**22**) only the reaction with the gold phosphine cations led to the isolation of **23** and **24.** The products of the reaction with the copper and silver phosphine cations decomposed quickly and as a result could not be identified.[29]

The syntheses of all isolated double and triple clusters were identical. A solution of the clusters (**1**, **2**, or **22**) in THF or CH_2Cl_2 was reacted with 1/2 equiv of metal phosphine cation. The reaction was complete within minutes, indicated by a color change to deep red. By addition of hexane the cationic bi/trifunctional clusters were isolated quantitatively (Figure 4).

With all of the described bifunctional phosphines, heterometallic double clusters of the half-sandwich type I were synthesized. While the resulting copper and gold clusters could be isolated in high yields, the reactions with the silver compounds were often incomplete and resulted in decomposition products. Table 2 shows all the compounds that have been synthesized in this project.

(29) Imhof, D. Thesis, ETH 10850, 1994.

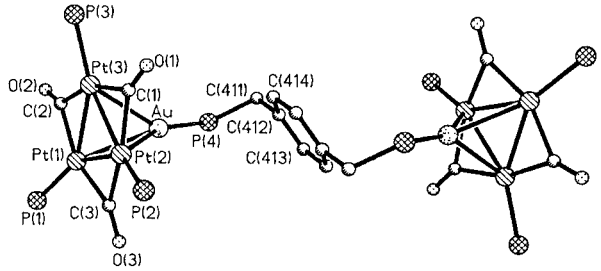

Figure 5. ORTEP view of **14**, showing the core atoms.

Discussion

The stability of the heterometallic platinum clusters can be correlated with the Lewis acidity strength of the metal cations. Thus the most acidic Au^+ ($pK_{hyd.} < 4$) coordinates stronger than the less acidic Cu^+ and Ag^+ ($pK_{hyd.}$ *ca.* 6.9).[30] The following order has been determined empirically from the tendency of formation and stability of the obtained compounds: $Au^+ > Cu^+ > Ag^+$.

In this context the behavior of the sandwich clusters of type II toward metal hydrides emphasizes this trend. While the gold compounds do not undergo any reaction, both copper and silver sandwich clusters react completely to form new hydride clusters.[31]

The behavior of the double and triple clusters is almost identical to that of the half-sandwich type I. In this case we observed that the gold and copper half-sandwich clusters are more stable than the analogous silver compounds. The latter decompose slowly in solution to the thermodynamically more stable sandwich compounds of type II.

X-ray Structure Determination. Small bright rhombohedron-shaped crystals of the double cluster cation $[\{Pt_3(\mu\text{-CO})_3(PCy_3)_3\}_2\{(AuPPh_2)_2(CH_2)_2C_6H_4\}]^{2+}$ (**14**) have been obtained by slow diffusion of cyclohexane into a solution of **14** in chloroform. An ORTEP view of **14** of the core atoms is shown in Figure 5. Selected bond lengths and bond angles are given in Table 3, and a full list can be found in the Supporting Information.

The X-ray crystal structure of **14** reveals that this compound consists of discrete Pt−Au cations and PF_6^- anions. The gold atom caps the triangular Pt_3 unit forming a slightly distorted Pt_3Au tetrahedron with Au−Pt distances between 2.7666(13) and 2.7283(10) Å at 150 K. These values Pt-Au distances of 2.750−2.768 Å are within the same range as those for $[\{Pt_3(\mu\text{-CO})_3(PCy_3)_3\}\{AuPCy_3\}]^+$ (**33**).[6]

Similary, the Pt−Pt bond lengths are comparable for both compounds **14** and **33**, with average Pt−Pt bond length of 2.666(1) and 2.682(9) Å, respectively. However, due to the coordination of the gold phosphine cation to $[Pt_3(\mu\text{-CO})_3(PCy_3)_3]$, an average lengthening of the Pt−Pt bond of 0.02 Å for the

(30) Yatsimirskii, K. B.; Wassiljew, V. P. *Instability Constants of Complex Compounds*; Pergamon Press: Elmsford, N.Y, 1960.
(31) Imhof, D.; Fadini, L.; Dahmen, K.-H.; Venanzi, L. M. Publication in preparation.

Table 3. Selected Bond Lengths (Å) and Bond Angles (deg) of **14** and **33**

	14	**33**		**14**	**33**
		Bond Lengths			
Pt(1)−Pt(2)	2.6644(8)	2.663(1)	Pt−P(av)	2.274(3)	2.273(1)
Pt(1)−Pt(3)	2.6701(13)	2.670(3)	Pt(1)−C(2)	2.08(2)	2.047(1)
Pt(2)−Pt(3)	2.6627(8)	2.663(1)	Pt(2)−C(3)	2.04(2)	2.046(1)
Pt(1)−Au	2.7666(13)	2.765(1)	Pt(3)−C(1)	2.074(14)	2.057(1)
Pt(2)−Au	2.7283(10)	2.728(1)	C−O(av)	1.18 (2)	1.182(1)
Pt(3)−Au	2.7333(12)	2.733(1)			
		Angles			
Pt(1)−Pt(2)−Pt(3)	60.16(3)	60.2(0)	Pt(3)−Pt(1)−Pt(2)	59.89(3)	59.9(0)
Pt(1)−Pt(3)−Pt(2)	59.95(3)	59.9(0)	Pt(1)−Au−Pt(2)	58.01(2)	58.0(0)

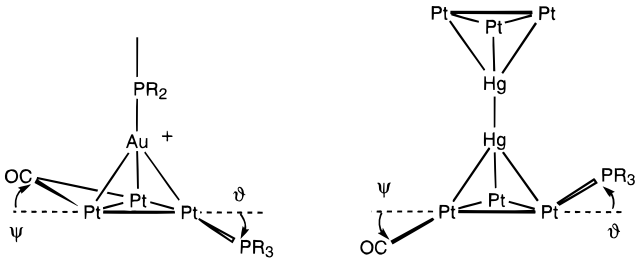

Figure 6. Torsion angles of the ligands to the Pt_3 plane of the tetrahedral gold cluster **11** and the mercury cluster.

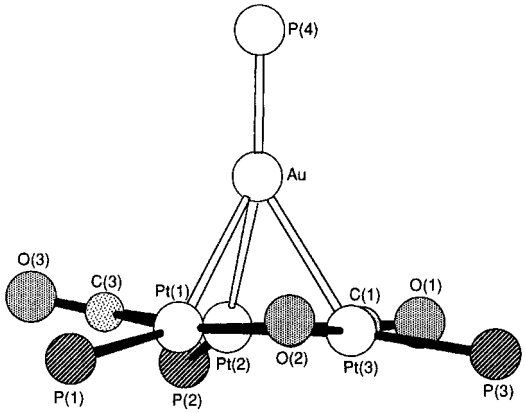

Figure 7. Projection of the Pt_3 plane in **11**.

double cluster **14** and 0.035 Å for the half-sandwich cluster **33**,[6] with respect to the uncoordinated cluster, can be observed. These differences might be directly related to the different Lewis basicities of the phosphine (in **14** the arylphosphine is less basic than the alkylphosphines in **33**) that is coordinated at the gold atom.

A look at the changes in the torsion angles of the ligands to the Pt_3 plane is interesting. In the uncoordinated cluster **1**, both the phosphine and carbonyl ligands are bent by an average angle of 15° out of the Pt_3 plane (Figure 6) in opposite directions to each other.[32] The coordination of the gold phosphine cation changes the positions of the ligands. While the phosphines are bent with an average angle of 20° away from the Pt_3 plane from the gold phosphine cation, the carbonyl ligands are almost in plane (Figure 7).

These torsion angles are not equal for all ligands. For the double cluster **14**, one of the three CO ligands is bent away by 3° more than the others and one of the PR_3 ligands is bent by 9−10° closer toward the Pt_3 plane than the other two (Table 4). This behavior is exactly contrary to that seen in the mercury(0) clusters where the phosphines are bent toward the metal and the carbonyl ligands are bent away from the metal (Figure 6).[16] This confirms the different type of interaction that has been reported in the mercury(0) adduct clusters.[33]

The FAB(+) MS is a very useful tool for the verification of the predicted structure of this large cluster. The parent peak is that of the cluster cation ($[MPF_6]^+$). The contribution of isotopes can be simulated and used as a fingerprint for the identification of the cluster structure. This helped us to identify the ferrocenyl−platinum cluster $[\{[1,1'\text{-}(AuPPh_2)_2Fe(\eta\text{-}C_5H_5)_2\}\text{-}\{Pt_3(\mu_2\text{-}CO)_3(PCy_3)_3\}_2][PF_6]_2$ (**27**), sketched schematically in Figure 8. Although this compound crystallizes easily, all attempts failed in obtaining suitable crystals for X-ray diffraction.

IR Spectroscopy. The changes in the electronic structure of the $[Pt_3(\mu\text{-}CO)_3(PR_3)_3]$ unit caused by addition of Lewis acids are shown in the ν(CO) frequencies in the IR spectra and in the ^{31}P-NMR data. In the IR spectra, the CO frequencies of the double cluster are at 1798−1800 cm^{-1} (st) and 1768−1787 cm^{-1} (m). Compared to the free cluster **1** (ν(CO) = 1764, 1738 cm^{-1}), a shift of 30 cm^{-1} to higher frequencies can be observed.

Compared to the free cluster $[Pt_3(\mu\text{-}CNXyl)_2(\mu\text{-}CO)(CNXyl)\text{-}(PCy_3)_2]$ (**2**), the same behavior can also be observed for the terminal isonitrile ligand and the bridging carbonyl ligand of the addition products **8** and **20** with a shift toward higher frequencies of 20 and 40 cm^{-1}, respectively.

The trend of shifting to higher frequencies by the coordination of a metal fragment to the building block Pt_3 would suggest a weakening of the π-back-bonding from the platinum to the carbonyl ligand which would cause a lengthening of the M−CO bond and a strengthening of the C−O bond. However, such bond length changes cannot be confirmed by the X-ray structure. In **14** the C−O bond lengths are almost equal to those in **1**, and those in **33** are even longer (1.28(2) *vs* 1.19(4)).[6] A possible explanation might be the change of the torsion angles discussed above and the possible dynamics of carbonyl ligands in the cluster. A correlation between the IR shift frequencies and the C−O bond length cannot be easily given.

NMR Spectroscopy. All of these compounds give a characteristic pattern in $^{31}P\{^1H\}$-NMR spectroscopy caused by the arrangement of the active isotopes ^{195}Pt (natural abundance, na = 33.7%) and ^{31}P (na = 100%) in the cluster skeleton. The exact explanation of the NMR patterns of $[Pt_3(\mu\text{-}CO)_3(PR_3)_3]$, $[Pt_3(\mu\text{-}CNR)_2(\mu\text{-}CO)(CNR)(PR_3)_2]$, and $[Pt_3(\mu\text{-}CNR)_3(CNR)_2\text{-}(PR_3)]$ is given in the references. However, in order to understand the ^{31}P-NMR spectrum shown in Figure 9, we give a brief explanation here.

The spectrum of the $[Pt_3(\mu\text{-}CO)_3(PCy_3)_3]$-unit **1** is mainly a linear combination of the signals of two of the isotopomers with the highest natural abundance A_3 and $A_2A'X$.[7] By substitution of one phosphine and two carbonyl ligands in **1** with isonitrile ligands, the cluster $[Pt_3(\mu\text{-}CNXyl)_2(\mu\text{-}CO)(CNXyl)(PCy_3)_2]$ (**2**) is formed. The symmetry of the system decreases from D_{3h} to C_{2v}. Therefore the number of possible isotopomers increases from 4 to 6.[2,34] The spin systems of the most important

(32) Albinati, A. *Inorg. Chim. Acta* **1977**, *22*, L31.

(33) Gade, L. H. *Angew. Chem., Int. Ed. Engl.* **1993**, *32*, 24.

Table 4. Torsion Angles (deg) of the Phosphine and Carbonyl Ligands of **1**, **14**, and **33**[32]

torsion angles (χ)	**1**	**33**	**14**	torsion angles (φ)	**1**	**33**	**14**
Pt(1)−Pt(2)−Pt(3)−C(1)	16.5	5.8	2.6	Pt(2)−Pt(3)−Pt(1)−P(1)	−15.5	−20.9	−25.3
Pt(1)−Pt(2)−Pt(3)−C(2)	7.6	1.6	1.8	Pt(1)−Pt(3)−Pt(2)−P(2)	−13.3	−20.4	−27.7
Pt(1)−Pt(3)−Pt(2)−C(3)	18.2	0.8	5.4	Pt(1)−Pt(2)−Pt(3)−P(3)	−18.2	−17.4	−15.1

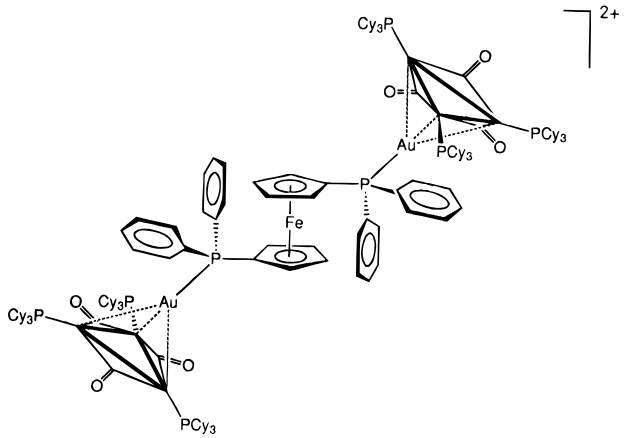

Figure 8. Schematic Drawing of [{[1,1′-(AuPPh$_2$)$_2$Fe(η-C$_5$H$_5$)$_2$}{Pt$_3$-(μ_2-CO)$_3$(PCy$_3$)$_3$}$_2$][PF$_6$]$_2$ (**27**).

isotopomers are A$_2$, AA′X, and A$_2$X. Further substitution of one CO and one PR$_3$ in **2** forms the cluster [Pt$_3$(μ-CNXyl)$_3$-(CNXyl)$_2$(PCy$_3$)] (**22**). Due to the single phosphorus atom in **22**, the subspectra of the isotopomers are exclusively of first order and the spectrum can be easily interpreted.[2,34]

By the coordination of the metal phosphine cation, an additional phosphorus is introduced which leads to a further splitting of the signals in the spectra. This gives additional information about the structure in solution and about the bonding of the metal fragment to the cluster. For all the gold compounds a quartet with platinum satellites is found. This points out that the gold phosphine unit is bonded symmetrically to the Pt$_3$ triangle forming a Pt$_3$Au tetrahedron. Due to the structural symmetry of the gold double clusters, with a C_3 axis mirror plane or an inversion center, both Pt$_3$Au tetrahedrons are chemically equivalent and do not differ in the NMR spectrum. Therefore the spectra are almost identical to those of the half-sandwich compounds.[6] This is also the case for the copper and silver compounds.

The situation in the ^{31}P-NMR spectra of the copper analogues is identical. However due to the fact that the natural isotopes ^{63}Cu and ^{65}Cu have spin $I = {}^3/_2$ and a high electromagnetic moment, the signals are broadened, especially the signal of the phosphorus that is directly bonded to the copper atom. The determination of all coupling constants is therefore not easy to achieve.

The fact that silver has two NMR active isotopes, ^{107}Ag (51.84%) and ^{109}Ag (48.16%) with spin $I = +{}^1/_2$ leads in the ^{31}P{^{1}H}-NMR spectrum of the silver addition products to a further splitting of the NMR pattern discussed above (Figure 9). For example, in the simple case without NMR-active platinum, the phosphine on the silver (P$_M$) gives rise to two doublets of quartets caused by the coupling to one of the silver isotopes and the three phosphorous atoms of the Pt$_3$ unit. Because ^{109}Ag has the higher gyromagnetic moment compared to ^{107}Ag, all signals of this mutliplet are split twice.

In a comparison of the double cluster and the half-sandwich clusters, only slight but significant changes in the chemical shift and coupling constants of the NMR spectra can be seen (Table 5). One reason for this behavior is certainly the fact that the basic unit is always the same and the changes can only be affected by the coordinated groups. The other reason is the organic groups are in general too large for sufficient spin−spin interaction of one cluster unit to the other.

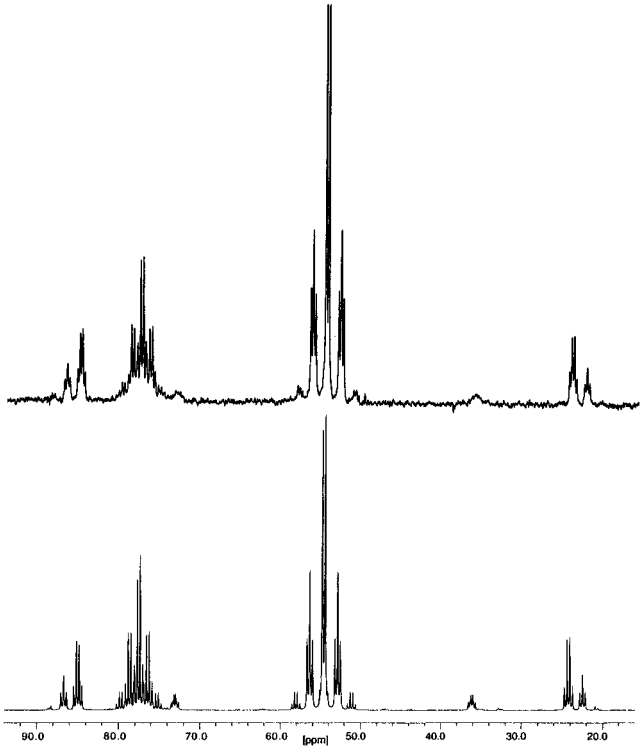

Figure 9. ^{31}P{^{1}H}-NMR spectrum of **16**: (Top) experimental spectrum; (bottom) simulated spectrum.

Because the building block [Pt$_3$(μ-CO)$_3$(PCy$_3$)$_3$] (**1**) remains the same for all of the synthesized half-sandwich- and double-cluster compounds described here, the influence of the electronegativity of the metal fragment MPR$_3^+$ on the ^{31}P-chemical shifts δ and coupling constates can be studied. The phosphorus of the Pt$_3$ unit (P) and the phosphorus of the added metal fragment MPR$_3$ (P_M) have different chemical shifts. The chemical shifts $\delta(P)$ of the cluster phosphines move approximately 10−12 ppm upfield upon coordination of a metal fragment MPR$_3^+$ and are not strongly influenced by the different metals in the MPR$_3^+$ unit. In the case of the ^{31}P-NMR chemical shifts $\delta(P^*)$ the effects of the R groups are even more pronounced and show a strong relationship with the following metal ions: Cu$^+$, Ag$^+$, Au$^+$.

The change in the electronic structure of the Pt$_3$-cluster unit caused by "addition" of the other metal fragments is clearly shown by comparing the ^1J(Pt,P) coupling constants. The ^1J(Pt,P) values are significantly larger for the heterometallic clusters than for the uncoordinated clusters (4670−4870 Hz *vs* 4410 Hz). An increase of the ^1J(Pt,P) for MPR$_3^+$ (R = Ph, Cy) follows the order Cu$^+$ > Ag$^+$ > Au$^+$. In general the ^1J(Pt,P) values of the same compounds are larger for the phenyl-containing MPR$_3^+$ (M = Cu$^+$, Ag$^+$) than for those containing cyclohexyl groups. A more precise analysis of the NMR data is given in the Supporting Information.

(34) Briant, C. E.; Gilmour, D. I.; Mingos, D. M. P.; Wardle, R. W. M. *J. Chem. Soc., Dalton Trans.* **1985**, 1693.

Table 5. $^{31}P\{^1H\}$-NMR Data for all Double and Triple Clusters

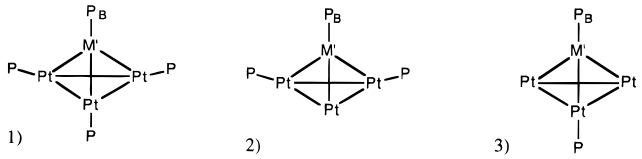

cmpd	δ_P	δ_{P_M}	^1J(Pt,P)	^2J(Pt,P)	^2J(Pt,PM)	^3J(P,P′)	^3J(P,PM)	^1J(Pt,Pt′)	^1J(Ag,PM)	^2J(Ag,P)
1[1]	69.8		4412	430		58		−1548		
2[2]	71.3		4102	435/439		56		−1050/−325		
3[1]	58.3	53.2	4673	303	122	31	11.3	−2080		
4[1]	59.4	65.6	4797	286	139	28	10.5	−2010	605/524	28/28
5[1]	58.1	55.5	4877	257	230	25	25	−2050		
6[2]	56.0	51.1	4456	332/302	131/131	33	11.1	−1990		
7[2]	58.8	54.5	4501	304/271	120/120	23.5	7.7	n.o.	651/564	27/27
8[2]	54.8	52.7	4699	284/258	217/217	23.5	22.4	−1950		
9[1]	56.0	51.2	4659	303	123	30	10.2	−1887		
10[1]	57.0	64.8	4766	285	138	26.6	10.8	n.o.	551/477	28/28
11[1]	56.2	83.9	4904	272	189	26	26	−2080		
12[1]	56.1	51.1	4669	303	127	30.7	11.2	−1944		
13[1]	57.0	63.1	4782	288	144	28.2	10.5	n.o.	588/510	28/28
14[1]	55.9	59.2	4911	268	213	27.5	27.5	−2015		
15[1]	56.0	51.0	4664	303	106	32	11.3	−1975		
16[1]	56.9	63.0	4778	285	152	29	10.1	−1990	608/525	28/28
17[1]	54.6	77.5	4921	280	182	27	27	−2100		
18[2]	55.9	41.0	4414	333/303	138/138	33	10.3	n.o.		
19[2]	57.9	62.9	4521	316/283	129/129	28	9.5	n.o.	661/574	28/28
20[2]	53.6	62.9	4685	294/270	197/197	28	23.2	−1925		
21[1]	56.1	54.0	4875	256	240	25.2	25.2	−2030		
22[3]	58.3		3877	446						
23[3]	40.6	67.6	4411	321/321	238/274		15.1	n.o.		
24[3]	44.3	61.6	4442	313/313	223/298		16.7	n.o.		
25[1]	56.1	51.5	4668	303	119	31	10.7	−2075		
26[1]	56.9	63.0	4799	287	140	27.8	10.7	−2030	606/526	28/28
27[1]	52.2	52.8	4927	269	176	25.3	25.3	−2145		
28[1]	55.9	50.7	4727	315	127	30	12	n.b.		
29[1]	56.9	62.8	4791	305	149	29	10.5	−2068	624/	27/27
30[1]	59.1	55.7	4868	260	235	25	25	−2020		
31[1]	56.0	51.0	4657	307	121	28.7	10.0	−1986		
32[1]	56.9	63.0	4776	286	138	28	9.3	−1875	572/	26/26
33[1]	51.9	82.7	4899	282	177	25	25	−2100		
34[2]	56.8	41.5	4453	335/312	125/125	34.5	8.5	n.b.		
35[2]	59.7	55.3	4506	315/284	135/135	28	7.5	n.b.	627/553	28/28
36[2]	55.9	78.4	4665	301/271	179/179	29.5	20.5			
37[3]	45.9	73.2	4401	323/237	270/270		20			

Summary and Conclusions

Platinum carbonyl phosphine cluster of the type $[Pt_3(\mu\text{-}CO)_3(PR_3)_3]$ react with polyfunctional d^{10} metal phosphine cations $[(MPR'_2)_n(R'')]^{n+}$ ($n = 2, 3$; $R'' = C_6H_4$, $(CH_2)_2C_6H_4$; M = Cu, Ag, Au) to form double and triple clusters $[\{Pt_3(\mu\text{-}CO)_3(PR_3)_3\}_n\{(MPR'_2)_n(R'')\}]^{n+}$ ($n = 2, 3$). The crystal structure of $[\{Pt_3(\mu\text{-}CO)_3(PCy_3)_3\}_2\{(AuPPh_2)_2(CH_2)_2C_6H_4)\}][PF_6]_2$ shows one representative of this new class of compounds. Their reactivity and stablity is very similar to that of the corresponding half-sandwich clusters $[\{Pt_3(\mu\text{-}CO)_3(PCy_3)_3\}\{(MPR'_3\}]^+$.

Although the platinum isonitrile carbonyl phosphine clusters of the type $[Pt_3(\mu\text{-}CNXyl)_2(\mu\text{-}CO)(CNXyl)(PR_3)_2]$ allow the synthesis of the copper, silver, and gold double clusters, only the gold double cluster was obtained for the platinum isonitrile phosphine clusters of the type $[Pt_3(\mu_2\text{-}CNXyl)_3(CNXyl)_2(PR_3)\}_2]$.

Due to the high symmetry of all these clusters the spectroscopic data are very similar. No large differences between the chemical shifts or coupling constants of the phenyl- and benzyl-containing bridging ligand were found that would lead to the conclusion of a possible delocalized electron conjugated system. The differences found are mainly caused by the differences in the Lewis acidity of the metal center as well as by the Lewis basicities of the phosphines on the platium cluster. These effects are similar to those observed for the corresponding half-sandwich compounds.

Experimental Section

Reactions were routinely carried out using standard Schlenk line procedures under an atmosphere of pure argon and using dry O_2-free solvents. The compounds $[1,4\text{-}(PPh_2)_2C_6H_4]$ (**38**),[22] $[1,3,5\text{-}(PPh_2)_3C_6H_3]$ (**42**),[22] $[1,1'\text{-}(PPh_2)_2Fe(\eta\text{-}C_5H_5)_2]$ (**43**),[35] $[Au(PPh_3)Cl]$,[22] $[Au(PCy_3)Cl]$-22, $[1,4\text{-}(AuClPPh_2)_2C_6H_4]$ (**44**),[22] $[1,1'\text{-}(AuClPPh_2)_2Fe(\eta\text{-}C_5H_5)_2]$ (**49**),[36] $[Pt_3(\mu\text{-}CO)_3(PCy_3)_3]$ (**1**),[37] $[Pt_3(\mu\text{-}CNXyl)_2(\mu\text{-}CO)(CNXyl)(PCy_3)_2]$ (**2**),[34] and $[Pt_3(\mu\text{-}CNXyl)_3(CNXyl)_2(PCy_3)]$ (**22**)[34] were prepared as described in the literature**.** Infrared spectra were recorded on a Perkin-Elmer 883 spectrometer as RbI pellets. $^{31}P\{^1H\}$-NMR spectra were run on a Bruker AC250 spectrometer. The ^{31}P operating frequency was 101.3 MHz. $^{31}P\{^1H\}$-NMR were measured and reported using H_3PO_4 (85%) as an internal standard and Na_2PtCl_6, respectively. $^{31}P\{^1H\}$-NMR simulations were carried out using a program developed by A. K. Rappe.

Preparation of 1,4-*Bis(*dicyclohexylphosphino)benzene (39). *p*-Dibromobenzene (1.82 g, 7.73 mmol) was dissolved in Et_2O (20 mL).

(35) Bishop, J. J.; Davison, A.; Katcher, M. L.; Lichtenberger, D. W.; Merrill, R. E.; Smart, J. C. *J. Organomet. Chem.* **1971**, *27*, 241.
(36) Hill, D. T.; Girard, G. R.; McCabe, F. L.; Johnson, R. K.; Stupik, P. D.; Zhang, J. H.; Reiff, W. M.; Eggleston, D. S. *Inorg. Chem.* **1989**, *28*, 3529.
(37) Moor, A.; Pregosin, P. S.; Venanzi, L. M. *Inorg. Chim. Acta* **1981**, *48*, 153.

A solution in hexane of *n*-BuLi (19.3 mL, 30.94 mmol) (1.6 M) was slowly added at 0 °C. The resulting solution was vigorously stirred for 2.5 h at 60 °C. After the solution was cooled to 0 °C, dicyclohexylchlorophosphine (3.74 mL, 17.01 mmol) was added dropwise, and the resulting solution was heated for 5 h and hydrolyzed with MeOH/H_2O. The resulting solid was isolated and washed with H_2O, MeOH, and Et_2O to give white crystals of **39** in 22% yield. Anal. Calcd for $C_{30}H_{48}P_2$: C, 76.56; H, 10.28. Found: C, 74.91; H, 10.38. IR: 2919 vs, 2849 vs, 1443 s, 1371 w, 1343 w, 1262 w, 1177 m, 1110 m, 995 m, 884 m, 851 m, 813 m, 538 m, 512 m. ^{1}H-NMR: 7.6−7.2 (m, 4 H); 2.1−1.5 (m, 24 H); 1.5−0.8 (m, 20 H). $^{31}P\{^1H\}$-NMR: δ(P) = 2.0 (s).

Preparation of Bis(diphenylphosphino)-*p*-xylene (40). Diphenylchlorophosphine (4.86 mL, 26.29 mmol) was dissolved in thf (25 mL). After the solution was cooled to 0 °C, small pieces of lithium (400 mg, 57.60 mmol) were added. After 2 h the excess of lithium was filtered off and the red solution was added dropwise to a solution of α,α′-dibromo-*p*-xylene (3.2 g, 12.12 mmol) in thf (20 mL). After being heated for 4 h, the mixture was hydrolyzed, filtered, and washed with H_2O, MeOH, and Et_2O to give white crystals in 37% yield. Concentration and cooling of the filtrate resulted in a total yield of 52%. Anal. Calcd for $C_{32}H_{28}P_2$: C, 81.00; H 5.95. Found: C, 80.25; H 6.01. IR: 3062 w, 3022 w, 1582 w, 1505 m, 1475 m, 1427 m, 1082 w, 1063 w, 847 m, 825 m, 737 s, 694 vs, 526 s, 505 m, 460 w, 416 w. ^{1}H-NMR: 7.75−7.25 (m, 24 H); 3.34 (s, 2 CH_2P). $^{31}P\{^1H\}$-NMR: δ(P) = −11.1 (s).

Preparation of Bis(dicyclohexylphosphino)-*p*-xylene (41). Dicyclohexylchlorophosphine (3.1 g, 15.63 mmol) was dissolved in Et_2O (30 mL). A solution of *n*-BuLi (10.3 mL 16.50 mmol) in hexane (1.6 M) was slowly added at 0 °C with vigorous stirring. The solution was allowed to continue to stir for 30 min at room temperature. After dropwise addition of α,α′-dibromo-*p*-xylene (2.0 g, 7.8 mmol) in thf (25 mL), the solvent was removed by distillation and the resultant solid hydrolyzed with H_2O (50 mL) and extracted with CH_2Cl_2 (30 mL). Crystallization from CH_2Cl_2/MeOH gave white crystals in 17% yield. Anal. Calcd for $C_{32}H_{52}P_2$: C, 77.07; H 10.51. Found: C, 75.70; H, 10.51. IR: 2924 vs, 2847 vs, 1508 s, 1443 s, 1264 m, 1220 m, 1173 m, 1104 m, 1020 m, 998 m, 887 m, 842 s, 810 s, 539 sh, 515 m. $^{31}P\{^1H\}$-NMR: δ(P) = 2.0 (s).

General Preparation of [Phosphine]bis[chlorogold]. $NaAuCl_4 \cdot 2H_2O$ (1.22 mmol) was dissolved in MeOH (20 mL) at 0 °C, and thiodiglycine (5.50 mmol) in MeOH (4 mL) was added. Once the solution turned colorless (ca. 20 min), bis(phosphine) (0.61 mmol) in CH_2Cl_2 (or $CHCl_3$) (20 mL) was added. After warming to room temperature and stirring for 2 h, the CH_2Cl_2 was removed. The resultant solid was filtered out and washed with MeOH to give white crystals in 85−100% yield.

[1,4-Bis(dicyclohexylphosphino)benzene]bis[chlorogold] (45). Anal. Calcd for $C_{30}H_{48}Au_2Cl_2P_2$: C, 38.52; H 5.17. Found: C, 38.57; H 5.26. IR: 2926 vs, 2849 s, 1444 m, 1379 m, 1347 w, 1297 w, 1267 w, 1201 w, 1176 w, 1119 m, 1003 m, 916 w, 888 w, 851 w, 819 m, 753 m, 559 s, 522 m, 328 m. ^{1}H-NMR: 7.85−7.70 (m, 4 H); 2.35−1.00 (m, 44 H). $^{31}P\{^1H\}$-NMR: δ(P) = 50.8 (s).

[α,α′-Bis(diphenylphosphino)-*p*-xylene]bis[chlorogold] (46). Anal. Calcd for $C_{32}H_{28}Au_2Cl_2P_2$: C, 40.92; H, 3.00. Found: C, 40.26; H, 3.10. IR: 3051 m, 3019 w, 2995 w, 2913 w, 1507 m, 1479 m, 1433 s, 1411 m, 1309 w, 1222 w, 1166 w, 1100 s, 1024 w, 997 w, 839 s, 746 vs, 718 sh m, 693 vs, 535 s, 514 s, 491 m, 469 m, 435 w, 326 s. ^{1}H-NMR: 7.65−7.45 (m, 20 H); 6.86 (m, 4 H); 3.70 (d, $^2J(^1H,^{31}P)$ = 10.4 Hz, 4 H). $^{31}P\{^1H\}$-NMR: δ(P) = 33.3 (s).

[α,α′-Bis(dicyclohexylphosphino)-*p*-xylene]bis[chlorogold] (47). Anal. Calcd for $C_{32}H_{52}Au_2Cl_2P_2$: C, 39.89; H, 5.44. Found: C, 41.57; H, 5.51. IR: 2924 vs, 2848 s, 1508 m, 1443 s, 1419 w, 1297 w, 1268 w, 1204 w, 1175 w, 1111 w, 1088 w, 1003 w, 889 w, 853 m, 838 sh m, 536 m, 516 m, 321 s. ^{1}H-NMR: 7.40 (m, 4 H); 3.20 (d, $^2J(^1H,^{31}P)$ = 10.3 Hz, 4 H); 2.0−1.6 (m, 24 H); 1.6−1.1 (m, 20 H). $^{31}P\{^1H\}$-NMR: δ(P) = 47.4 (s).

[1,3,5-Tris(diphenylphosphino)benzene]tris[chlorogold] (48). Anal. Calcd for $C_{42}H_{33}Au_3Cl_3P_3$: C, 37.99; H, 2.50. Found: C, 38.81; H, 2.57. IR: 3064 m, 1667 w, 1604 m, 1586 s, 1476 m, 1455 m, 1423 s, 1310 sh m, 1291 s, 1179 m, 1124 s, 1096 s, 1025 w, 991 m, 878 m, 858 m, 747 s, 693 s, 672 m, 569 m, 543 m, 502 s, 461 m, 332 m. $^{31}P\{^1H\}$-NMR: δ(P) = 33.8 (s).

General Preparation of Double Copper Compounds. Bis(phosphine) $PR_2R'PR_2$ (9.93 mmol) and $[Cu(CH_3CN)_4]PF_6$ (19.86 mmol) were dissolved in CH_2Cl_2 (or thf) (5 mL). The mixture was added dropwise to a solution of $[Pt_3(\mu\text{-}CO)_3(PCy_3)_3]$ or $[Pt_3(\mu\text{-}CNXyl)_2(\mu\text{-}CO)(CNXyl)(PCy_3)_2]$ (9.93 mmol) in CH_2Cl_2 (5 mL). After stirring for 30 min, the solution was concentrated to 1 mL. Addition of hexane gave a red powder in 70−91% yield.

$[\{1,4\text{-}(CuPPh_2)_2C_6H_4)\}\{Pt_3(\mu_2\text{-}CO)_3(PCy_3)_3\}_2][PF_6]_2$ (3). Anal. Calcd for $C_{144}H_{222}Cu_2F_{12}O_6P_{10}Pt_6$: C, 44.52; H 5.76. Found: C, 45.75; H, 5.93. IR: ν(CO) = 1825 sh m, 1795 vs, 1765 m.

$[\{1,4\text{-}(CuPPh_2)_2C_6H_4)\}\{Pt_3(\mu_2\text{-}CO)(\mu_2\text{-}CNXyl)_2(CNXyl)(PCy_3)_2\}_2][PF_6]_2$ (6). Anal. Calcd for $C_{158}H_{210}Cu_2F_{12}N_6O_2P_8Pt_6$: C, 47.46; H, 5.29; N, 2.10. Found: C, 46.50; H, 5.10; N, 1.81. IR: ν(CN,term.) = 2135 s; ν(CN,μ), ν(CO) = 1772 s, 1724 m, 1732 s.

$[\{1,4\text{-}(CuPCy_2CH_2)_2C_6H_4)\}\{Pt_3(\mu_2\text{-}CO)(\mu_2\text{-}CNXyl)_2(CNXyl)(PCy_3)_2\}_2][PF_6]_2$ (18). Anal. Calcd for $C_{160}H_{238}Cu_2F_{12}N_6O_2P_8Pt_6$: C, 47.44; H, 5.92; N, 2.08. Found: C, 46.11; H, 5.75; N, 1.78 IR: ν(CN,term.) = 2136 s; ν(CN,μ_2), ν(CO) = 1771 s, 1720 m.

$[\{[1,1'\text{-}(CuPPh_2)_2Fe(\eta\text{-}C_5H_5)_2\}\{Pt_3(\mu_2\text{-}CO)_3(PCy_3)_3\}_2][PF_6]_2$ (25). Anal. Calcd for $C_{148}H_{226}Cu_2F_{12}FeO_6P_{10}Pt_6$: C, 44.52; H 5.71. Found: C, 45.63; H, 6.11. IR: ν(CO) = 1794 st, 1767 m.

General Preparation of Double Silver Compounds. $PR_2R'PR_2$ (9.93 mmol) and $AgCF_3SO_3$ (19.86 mmol) were dissolved in CH_2Cl_2 (or thf) (5 mL). The mixture was dropwise added to a solution of $[Pt_3(\mu\text{-}CO)_3(PCy_3)_3]$ or $[Pt_3(\mu\text{-}CNXyl)_2(\mu\text{-}CO)(CNXyl)(PCy_3)_2]$ (9.93 mmol) in CH_2Cl_2 (5 mL). The solution immediately turned dark red. After stirring for 30 min, the solution was concentrated to 2 mL. Addition of hexane gave a deep-red powder in 53−70% yield.

$[\{1,4\text{-}(AgPPh_2)_2C_6H_4)\}\{Pt_3(\mu_2\text{-}CO)_3(PCy_3)_3\}_2][CF_3SO_3]_2$ (4). Anal. Calcd for $C_{146}H_{222}Ag_2F_6O_{12}P_8Pt_6S_2$: C, 44.04; H, 5.62. Found: C, 44.19; H, 6.24. IR: ν(CO) = 1793 vs, 1765 m.

$[\{1,4\text{-}(AgPPh_2)_2C_6H_4)\}\{Pt_3(\mu_2\text{-}CO)(\mu_2\text{-}CNXyl)_2(CNXyl)(PCy_3)_2\}_2][CF_3SO_3]_2$ (7). Anal. Calcd for $C_{160}H_{210}Ag_2F_6N_6S_2O_8P_6Pt_6$: IR: ν(CN,term.) = 2115 s; ν(CN,μ_2), ν(CO) = 1768 s, 1720 m.

$[\{1,4\text{-}(AgPCy_2CH_2)_2C_6H_4)\}\{Pt_3(\mu_2\text{-}CO)(\mu_2\text{-}CNXyl)_2(CNXyl)(PCy_3)_2\}_2][CF_3SO_3]_2$ (20). Anal. Calcd for $C_{162}H_{238}Ag_2F_6N_6S_2O_8P_6Pt_6$ IR: ν(CN,term.) = 2120 s; ν(CN,μ_2), ν(CO) = 1771 s, 1723 m.

$[\{[1,1'\text{-}(AgPPh_2)_2Fe(\eta\text{-}C_5H_5)_2\}\{Pt_3(\mu_2\text{-}CO)_3(PCy_3)_3\}_2][CF_3SO_3]_2$ (25). Anal. Calcd for $C_{150}H_{226}Ag_2F_6FeO_{12}P_8Pt_6S_2$: C, 44.06; H 5.57. Found: C, 44.52; H, 6.52. IR: ν(CO) = 1793 st, 1766 m.

General Preparation of Double Gold Compounds. $[ClAuPR_2R'PR_2AuCl]$ (0.016 mmol) and $TlPF_6$ (0.033 mmol) were dissolved in thf (2 mL). The mixture was added dropwise to a solution of $[Pt_3(\mu\text{-}CO)_3(PCy_3)_3]$, $[Pt_3(\mu\text{-}CNXyl)_2(\mu\text{-}CO)(CNXyl)(PCy_3)_2]$, or $[Pt_3(\mu\text{-}CNXyl)_3(CNXyl)_2(PCy_3)]$ (0.033 mmol) in CH_2Cl_2 (5 mL). After stirring for 10 min, the solution was concentrated. The resultant solid was dissolved in CH_2Cl_2, filtered through Celite, concentrated to 2 mL, and precipitated with hexane as deep-red crystals in 65−95% yield.

$[\{1,4\text{-}(AuPPh_2)_2C_6H_4)\}\{Pt_3(\mu_2\text{-}CO)_3(PCy_3)_3\}_2][PF_6]_2$ (5). Anal. Calcd for $C_{144}H_{222}Au_2F_{12}O_6P_{10}Pt_6$: C, 41.66; H 5.39. Found: C, 42.89; H, 5.62. IR: ν(CO) = 1798 vs, 1785 sh s.

$[\{1,4\text{-}(AuPCy_2)_2C_6H_4)\}\{Pt_3(\mu_2\text{-}CO)_3(PCy_3)_3\}_2][PF_6]_2$ (11). Anal. Calcd for $C_{144}H_{246}Au_2F_{12}O_6P_{10}Pt_6$: C, 41.42; H 5.94. Found: C, 41.50; H, 5.91. IR: ν(CO) = 1800 vs, 1770 m. MS (FAB$^+$): 4030 (100, $[MPF_6]^+$), 3946 (4, $[MPF_6 - CyH]^+$), 3885 (26, $[M]^+$), 3862 (20, $[MPF_6 - 2CyH]^+$), 2420 (10), 2093 (39), 1942 (49, $[M]^{2+}$), 1897 (10), 1858 (15), 752 (13), 751 (32, $[AuPCy_3PCy_2Ph]^+$), 749 (15).

High resolution MS (FAB$^+$, $[MPF_6]^+$): found, 4024.3 (13), 4025.3 (30), 4026.3 (50), 4027.3 (68), 4028.3 (87), 4029.3 (98), 4030.2 (100), 4031.3 (90), 4032.3 (75), 4033.3 (60), 4034.2 (40), 4035.2 (28), 4036.3 (18), 4037.1 (10), 4038.2 (7), 4039.3 (3); calcd, 4021 (0.26), 4022 (0.97), 4023 (3.18), 4024 (8.95), 4025 (20.66), 4026 (39.12), 4027 (61.70), 4028 (82.82),4029 (96.65), 4030 (100.00), 4031 (93.15), 4032 (79.05), 4033 (61.61), 4034 (44.41), 4035 (29.76), 4036 (18.62), 4037 (10.90), 4038 (5.99), 4039 (3.09), 4040 (1.50), 4041 (0.69), 4042 (0.30), 4043 (0.12).

$[\{1,4\text{-}(AuPPh_2CH_2)_2C_6H_4)\}\{Pt_3(\mu_2\text{-}CO)_3(PCy_3)_3\}_2][PF_6]_2$ (14). Anal. Calcd for $C_{146}H_{226}Au_2F_{12}O_6P_{10}Pt_6$: C, 41.96; H, 5.45. Found: C, 40.99; H, 5.34. IR: ν(CO) = 1800 vs, 1772 w. MS (FAB$^+$): 4034 (100, $[MPF_6]^+$), 3950 (6, $[MPF_6 - CyH]^+$), 3889 (25, $[M]^+$), 3866 (45, $[MPF_6$

− 2 CyH]$^+$), 2424 (7), 2097 (43), 1995 (24), 1944 (28, [M]$^{2+}$), 1860 (26), 1147 (11), 953 (16), 874 (14), 843 (10), 756 (10).

High resolution MS (FAB$^+$, [MPF$_6$]$^+$): found, 4028.4 (8),4029.4 (19), 4030.4 (46), 4031.4 (51), 4032.4 (75), 4033.4 (85), 4034.4 (100.00), 4035.4 (96), 4036.4 (86), 4037.5 (70), 4038.4 (60), 4039.4 (43), 4040.3 (26), 4041.3 (18); calcd, 4025 (0.26), 4026 (0.95), 4027 (3.14), 4028 (8.85),4029 (20.45), 4030 (38.79), 4031 (61.31), 4032 (82.47), 4033 (96.45), 4034 (100.00), 4035 (93.34), 4036 (79.37), 4037 (61.99), 4038 (44.77), 4039 (30.06), 4040 (18.84), 4041 (11.05), 4042 (6.09), 4043 (3.15), 4044(1.53), 4045 (0.7), 4046 (0.3), 4047(0.12).

[{1,4-(AuPCy$_2$CH$_2$)$_2$C$_6$H$_4$)}{Pt$_3$(μ_2-CO)$_3$(PCy$_3$)$_3$}$_2$][PF$_6$]$_2$ (17). Anal. Calcd for $C_{146}H_{250}Au_2F_{12}O_6P_{10}Pt_6$: C, 41.72; H, 5.99. Found: C, 41.58; H, 5.69. IR: ν(CO) = 1798 vs, 1768 m.

[{**1,3,5-(AuPPh$_2$)$_3$C$_6$H$_3$)}{Pt$_3$(μ_2-CO)$_3$(PCy$_3$)$_3$}$_3$][PF$_6$]$_3$ (21).** Anal. Calcd for $C_{213}H_{330}Au_3F_{18}O_9P_{15}Pt_9$: C, 41.34; H, 5.38. Found: C, 42.43; H, 5.26. IR: ν(CO) = 1799 vs, 1778 sh m.

[{1,4-(AuPPh$_2$)$_2$C$_6$H$_4$)}{Pt$_3$(μ_2-CO)(μ_2-CNXyl)$_2$(CNXyl)(PCy$_3$)$_2$}$_2$][PF$_6$]$_2$ (8). Anal. Calcd for $C_{158}H_{210}Au_2F_{12}N_6O_2P_8Pt_6$: C, 44.49; H, 4.96; N, 1.97. Found: C, 44.90; H, 5.19; N, 1.81. IR: ν(CN,term.) = 2134 s; n(CN,μ), ν(CO) = 1850 w, 1779 s, 1732 m, 1584 w.

[{1,4-(AuPCy$_2$CH$_2$)$_2$C$_6$H$_4$)}{Pt$_3$(μ_2-CO)(μ_2-CNXyl)$_2$(CNXyl)(PCy$_3$)$_2$}$_2$][PF$_6$]$_2$ (20). Anal. Calcd for $C_{160}H_{238}Au_2F_{12}N_6O_2P_8Pt_6$: C, 44.51; H, 5.56; N, 1.95. Found: C, 43.11; H, 5.55; N, 1.88. IR: ν(CN,term.) = 2132 s; ν(CN,μ_2), ν(CO) = 1852 sh w, 1778 s, 1728 s, 1585 m.

[{1,4-(AuPPh$_2$)$_2$C$_6$H$_4$)}{Pt$_3$(μ_2-CNXyl)$_3$(CNXyl)$_2$(PCy$_3$)}$_2$][PF$_6$]$_2$ (23). Anal. Calcd for $C_{156}H_{180}Au_2F_{12}N_{10}P_6Pt_6$: C, 44.89; H, 4.32; N, 3.36. Found: C, 45.15; H, 4.96; N, 3.18. IR: ν(CN) = 2132 vs; 1772 m, 1718 br s, 1584 m.

[{1,4-(AuPCy$_2$CH$_2$)$_2$C$_6$H$_4$)}{Pt$_3$(μ_2-CNXyl)$_3$(CNXyl)$_2$(PCy$_3$)}$_2$][PF$_6$]$_2$ (24). Anal. Calcd for $C_{158}H_{208}Au_2F_{12}N_{10}P_6Pt_6$: C, 44.91; H, 4.96; N, 3.31. Found: C, 45.20; H, 5.20; N, 3.04. IR: ν(CN) = 2124 vs, 1975 w, 1724 br s, 1584 m.

[{[1,1′-(AuPPh$_2$)$_2$Fe(η-C$_5$H$_5$)$_2$}{Pt$_3$(μ_2-CO)$_3$(PCy$_3$)$_3$}$_2$][PF$_6$]$_2$ (27). Anal. Calcd for $C_{148}H_{226}Au_2F_{12}FeO_6P_{10}Pt_6$: C, 41.73; H, 5.35. Found: C, 41.34; H, 5.18. IR: ν(CO) = 1799 st, 1769 m. MS (FAB$^+$): 4112 (100, [MPF$_6$]$^+$), 4029 (8, [MPF$_6$ − CyH]$^+$), 3968 (10, [M]$^+$), 3946 (66, [MPF$_6$ − 2 CyH]$^+$), 2420 (22), 2374 (48), 1992 (28), 1897 (78), 1226 (62), 954 (41), 875 (40), 751 (85).

High resolution MS (FAB$^+$, [MPF$_6$]$^+$): found, 4106.6 (6), 4107.6 (16), 4108.6 (30), 4109.6 (55),4110.8 (76), 4111 (95), 4112.6 (100), 4113.6 (96), 4114.6 (86), 4115.6 (77), 4116.6 (63), 4117.6 (48), 4118.6 (32), 4119.6 (19), 4120.6 (13), 4121.6 (8); calcd, 4106 (1.39), 4107 (4.09), 4108 (10.44), 4109 (22.56),4110 (41.00), 4111 (63.13), 4112 (83.61), 4113 (96.92), 4114 (100.00), 4115 (93.12), 4116 (79.13), 4117 (61.84), 4118 (44.73), 4119 (30.10), 4120 (18.92), 4121 (11.14), 4122 (6.16), 4123 (3.20), 4124(1.57), 4125 (0.72), 4126 (0.31), 4127(0.13).

X-ray Crystal Structure Analysis. Collection, Reduction, and Refinement of X-ray Data. Crystals of **14** were crystallized as described above from a mixture of chloroform and cyclohexane. A crystal, which showed no defects and a perfect extinction under polarized light, was drawn up with solvent into a glass capillary and mounted on a STOE IPDS scanner with an image plate detector for the determination of the lattice parameters and for the data collection. The lattice parameters were obtained by a pattern fit of 524 reflections in the range 6.3−45.0° collected at 4 different ϕ angles, which differ 45° from each other successively and thus yield a good selection of reciprocal space. Because of the unit cell contents and the approximately spherical shape of the crystal, an absorption correction did not seem necessary.

A total of 22 445 reflections were collected and 1459 were rejected because of boundary errors between different images. Intensities with $F < 5$ were cut off because the accuracy of the intensities was not sufficient according to several check measurements on a four-circle diffractometer (STOE STADI 4). Therefore 15 941 reflections were considered as observed, of which 8443 were independent and used for the structure determination and the final refinement of the structure.

Table 6. Crystallographic Data for [{Pt$_3$(μ-CO)$_3$(PCy$_3$)$_3$}$_2$}{(AuPPh$_2$)$_2$(CH$_2$)$_2$C$_6$H$_4$)}][PF$_6$]$_2$·2CHCl$_3$·2C$_6$H$_{12}$

chem formula = $C_{174}H_{278}O_6F_{12}P_{12}Cl_{12}P_{12}Pt_6Au_2$	space group = $P\bar{1}$
fw = 4993.54	$Z = 1$
a = 15.350(3) Å	δ =1.716 g/cm^3
b = 17.150(3) Å	μ = 6.148 mm^{-1}
c = 20.446(4) Å	T = −123 °C
α = 84.54(3)°	λ = 0.710 73 Å
β = 84.84(3)°	$R_w{}^a$ = 0.0990
γ = 64.56(3)°	R^b = 0.0435
V = 4831(2) Å^3	

^{a} w$R = (\sum w(F_o^2F_c^2)^2/\sum w(F_o^2)^2)^{1/2}$; $w = 1/(\sigma^2(F_o^2) + (aP)^2 + bP)$; $P = (F_o^2(\geq 0) + 2F_c^2)/3$. ^{b} $R = \sum||F_o| - |F_c||/\sum|F_o|$ (n = number of reflections; p = number of parameters).

The structure was solved by direct and Fourier methods using the SHELXTL PLUS[38] and SHELXL93[39] packages. Refinement was carried out by full-matrix least squares of 1000 parameters. The parameters of the solvent atoms were refined by rigid bond and similar displacement parameter restraints. Weighted R-factors wR and all goodness of fits are based on F^2 values. Conventional R-factors R are based on F values. (R-factors based on F^2 are in general about twice as large as conventional ones based on F.) The weighting function was $1/[\sigma^2(F^2) + (0.021P)^2 + 32.37P]$, with $P = [F_o^2 + 2F_c^2]/3$. Experimental and crystallographic details are shown in Table 6 and in the Supporting Information.

The cyclohexyl groups and the solvent molecules were to a certain extent disordered, which leads to large displacement parameters. An acentric model can be ruled out, because in this case the heavy atom parameters are strongly correlated and the data/parameter ratio becomes rather small. The positions of the hydrogen atoms were calculated by the default values of the SHELXL 93 program for 150 K, and the displacement parameters are 1.2 times as large as those of the corresponding nearest carbon atoms. These values were refined by riding the hydrogen parameters on the parameters of the carbon neighbors. The final atom coordinates and isotropic displacement parameters of the structure determination are given in the Supporting Information.

Acknowledgment. We are grateful for the financial support of the the Schweizerischen Schulrat (D.I., K.-H.D.) and the Bundesamt für Energiewirtschaft (F.J.). We gratefully acknowledge the use of the SHELXTL PLUS software of the Institut für Kristallographie of the ETH Zürich. We thank Dr. Amrein for the FAB measurements.

Supporting Information Available: NMR spectroscopy, including ^{31}P{^{1}H}-NMR spectra of **3** and **4** (Figures S1 and S2), δ(P) of double- and half-sandwich clusters as a function of different metals (Figure S3), ^1J(Pt,P) in half-sandwich and double clusters as a function of different metals (Figure S4), ^{31}P{^{1}H}-NMR data for phosphines, bi- and trifunctional gold phosphine chlorides, and clusters (Tables S1−S4) and Δ^1J(Pt,P) values (Table S5), and crystallography tables, including crystal data and structure refinement for **14**, atomic coordinates and equivalent isotropic displacement parameters, bond lengths and angles, anisotropic displacement parameters, and hydrogen coordinates and isotropic displacement parameters (Tables SS1−SS5) (26 pages). Ordering information is given on any current masthead page.

IC960846X

(38) SHELXLTL Plus Release 4.0, Siemens X-ray Instr. Inc., USA, 1990.
(39) SHELXL93: Sheldrick, G. M. Universität Göttingen, Germany, 1993.